

Article

Enhanced Nitrate Nitrogen Removal from Constructed Wetland via Fe₃O₄/Granular Activated Carbon Anode Microbial Electrolysis Cell under Low C/N Ratio

Heng Yang, Shenyu Tan, Yu Huang and Xinhua Tang *

School of Civil Engineering and Architecture, Wuhan University of Technology, Wuhan 430070, China; 262835@whut.edu.cn (H.Y.); tanshenyu@whut.edu.cn (S.T.); 320323@whut.edu.cn (Y.H.)

* Correspondence: tangxinhua@whut.edu.cn

Abstract: In this study, a constructed wetland–Fe₃O₄/granular activated carbon anode microbial electrolysis cell (CW-FMEC) was constructed to enhance denitrification in low COD/N ratio wastewater. The introduction of Fe₃O₄ boosted the expression of functional genes involved in the denitrification pathway, and the abundance of *narG*, *nirS*, and *nosZ* increased by 99.29%, 70.54%, and 132.18%, respectively, compared to CW. In addition, the content of c-type cytochromes (c-Cyts) and EPS were also enhanced in the CW-FMEC. The microbial communities study displayed that *Thauera*, *Dechloromonas*, and *Arenimonas* became the main genera for denitrification. The denitrification performance at different COD/N ratios was investigated in depth. Under optimal working circumstances, the CW-FMEC had an excellent nitrate removal rate (88.9% ± 1.12%) while accumulating nearly no NO₂[−]-N or NH₄⁺-N in the effluent. This study provides a new direction for the development of CW-MEC and accelerates its implementation.

Keywords: Fe₃O₄; CW-FMEC; denitrification pathway; low COD/N ratio; nitrate removal



Citation: Yang, H.; Tan, S.; Huang, Y.; Tang, X. Enhanced Nitrate Nitrogen Removal from Constructed Wetland via Fe₃O₄/Granular Activated Carbon Anode Microbial Electrolysis Cell under Low C/N Ratio. *Water* **2024**, *16*, 1377. <https://doi.org/10.3390/w16101377>

Academic Editor: Jesus Gonzalez-Lopez

Received: 13 April 2024

Revised: 8 May 2024

Accepted: 10 May 2024

Published: 11 May 2024



Copyright: © 2024 by the authors. Licensee MDPI, Basel, Switzerland. This article is an open access article distributed under the terms and conditions of the Creative Commons Attribution (CC BY) license (<https://creativecommons.org/licenses/by/4.0/>).

1. Introduction

Nitrogen, as an essential element for life, plays a vital role in the ecosystem material cycle and energy transfer. More and more human activities lead to excessive nitrogen discharge into natural water bodies, resulting in eutrophication and disrupting the ecosystem balance. Around 20% of the world's domestic water comes from groundwater, and nitrate nitrogen pollution is gradually becoming globalized due to the mobility of groundwater [1]. Nitrate transfer from water into the human body would also cause harm to the human body. Despite nitrate nitrogen itself having no direct harm on human bodies, it could result in diseases such as methemoglobinemia, endemic goiter, digestive system cancers [2]. Therefore, excessive nitrogen-containing pollutants in wastewater needed to be denitrified and converted into nitrogen before discharge [3].

The common techniques for removing nitrate nitrogen included physical, chemical, and biological methods [4]. However, the development of these nitrate reduction techniques has been limited due to limited adsorption capacity and non-renewability of adsorbents [5], difficulty of electro dialysis in treating complex wastewater [6], and susceptibility of reverse osmosis membranes to contamination [7]. Chemical methods such as catalytic reduction, active metal reduction, and electrochemical reduction have been slow to develop due to high costs and secondary pollution via by-products and are not in line with the concept of carbon neutrality. Biological denitrification, which refers to the process of reducing NO₃[−]-N to N₂ by microorganisms with a denitrification function, is superior to physical and chemical methods because of thorough reduction reaction, low secondary pollution, low cost, and high efficiency [8]. Zekker et al. [9] utilized real municipal wastewater supplied with CH₃COONa and KNO₃ and succeeded in the cultivation of biomass containing denitrifying polyphosphate-accumulating organisms (DPAOs). This biomass holds practical

potential for application in water treatment systems, effectively mitigating the inhibitory effects of nitrate on nitrite and demonstrating efficient nitrogen and phosphorus removal in their sequencing batch reactor (SBR) systems.

A constructed wetland (CW) is a kind of water treatment technology with low operating costs and high eco-efficiency [10], and has been successfully used to remove various pollutants, such as organic compounds, inorganic nutrients, and heavy metals, as well as having a relatively good treatment effect. Grinberga et al. [11] reported that efficient removal of phosphorus could be achieved by planting dense vegetation in constructed wetlands. However, a single constructed wetland had a rather limited treatment effect especially in the cases of low organic content and high nitrate nitrogen concentration. And, its nitrate removal performance was far from satisfactory when water was continually provided. Therefore, in the treatment of low carbon and nitrogen ratio wastewater, it is necessary to add carbon sources frequently, which not only improves costs but also produces a large amount of sludge and can even clog the wastewater treatment system, thereby reducing the treatment effect. With people having higher and higher requirements for wastewater treatment effectiveness, constructed wetlands coupled with other technologies have also attracted much attention [12]. The constructed wetland–microbial electrolysis cell (CW-MEC) has received widespread attention as a novel wastewater treatment and energy recovery technology. In the coupled system, plant root secretions could provide chemical energy for microorganisms, which could reduce the amount of externally added carbon sources, and the electrodes are also made of relatively cheap materials, which could reduce material costs in the separate MEC system. On the other hand, the constructed wetland with vertical flow provides a certain redox potential for MEC, which reduces the applied voltage and saves electrical energy. Therefore, the coupled CW-MEC system has better economic benefits and stronger pollutant removal ability, as well as better synthesis, stability, and more promising application prospects [13]. However, there is a limited number of studies on denitrification at a low COD/N ratio using constructed wetland–microbial electrolysis cell systems.

Fe_3O_4 is a suitable modifier and excellent material for supercapacitors due to its superior biocompatibility, unique $\text{Fd}3\text{m}$ structure, low cost, high bacterial affinity, and simple production. Through magnetic attraction, Fe_3O_4 particles make it easier to develop multilayer networks and accelerated electron transport [14]. It has been shown that Fe_3O_4 could also facilitate direct electron transfer between species [15]. In addition, some bacteria, such as *P. stutzeri*, were able to directly transfer Fe_3O_4 into their cells for growth and metabolism, without first breaking it down into dissolved Fe^{2+} and Fe^{3+} . On the other hand, by promoting growth and metabolism through direct contact with bacteria, Fe_3O_4 could increase the expression of electron-transfer-related proteins, such as NADH dehydrogenase and cytochrome *c* in adherent bacteria, thus increasing the overall number of bacteria in the system [16]. However, there is a limited number of studies focusing on improving the removal of nitrate nitrogen from constructed wetland microbial electrolysis cells using Fe_3O_4 -modified materials.

In this work, a coupled constructed wetland–microbial electrolysis cell system was established to evaluate the effect of nitrate denitrification under the condition of a low carbon ratio, and the optimal operating conditions were determined, based on which nanoscale Fe_3O_4 -modified granular activated carbon (GAC) was prepared as the three-dimensional anode of the system using a simple polytetrafluoroethylene (PTFE) adhesion method, which further improved the performance of the system. The microbial community in the system was identified via 16S rRNA sequencing, and the N-related functional genes were quantified using high throughput qPCR chip technology. Furthermore, the mechanism of electrical enhancement and anode modification enhancement was explored. This work provides theoretical support for the application of microbial electrolysis cells to improve the removal rate of nitrate nitrogen from a constructed wetland under the condition of a low COD/N ratio.

2. Materials and Methods

2.1. Synthesis of $\text{Fe}_3\text{O}_4/\text{GAC}$ Composite Particles

The previously described preparation method was modified to create the $\text{Fe}_3\text{O}_4/\text{GAC}$ composite particles [17]. Fe_3O_4 was purchased from Beasley New Materials (Suzhou) Co., Ltd. (Suzhou, China) with an average particle size of 200 nm. Figure 1 depicts the synthesis procedure. A homogenous suspension was prepared by ultrasonically blending a specific dosage of Fe_3O_4 (1.2 g), PTFE (5 g), isopropyl alcohol, and deionized water (50 mL) for 30 min. Subsequently, an appropriate quantity of GAC that could pass through an 8-mesh filter was immersed into the mixture and subjected to a sonication process for a period of 30 min. Following this, the GAC after hybrid ultrasound treatment was successively washed with deionized water and ethanol. The $\text{Fe}_3\text{O}_4/\text{GAC}$ composites were obtained by drying the final product in a vacuum oven at 80 °C for 24 h.

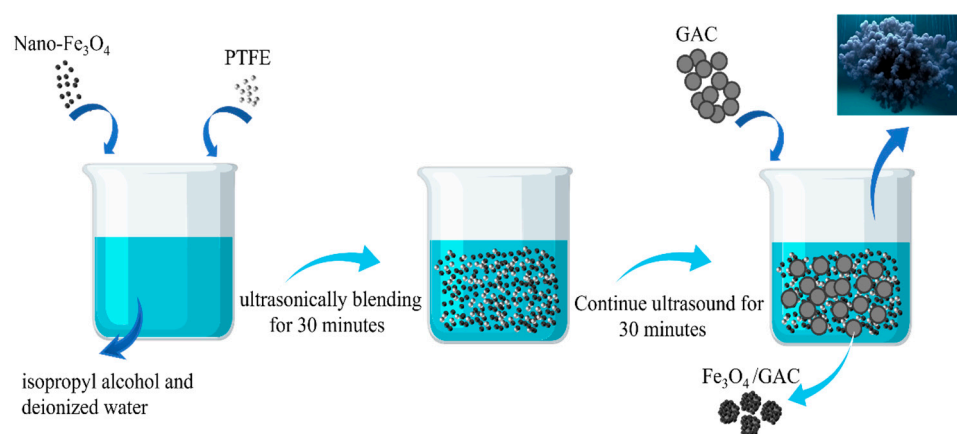


Figure 1. Preparation of $\text{Fe}_3\text{O}_4/\text{GAC}$ composite particles.

2.2. Experimental Start-Up

The schematic structure of the reactor is shown in Figure 2. Three wetland reactors were constructed using polyethylene plastic; each column was 50 cm high, 14 cm in diameter and, 5 mm thick. A gravel (6–13 mm) layer of 10 cm was placed at the bottom as a support layer. The anode of the CW-MEC consisted of graphite carbon felt with a width of 10 cm, a length of 15 cm, and a thickness of 5 mm, which was curled and placed in 2–4 mm coconut shell activated carbon to establish a three-dimensional anode system to enhance the mass transfer efficiency of the anode. The cathode, carbon felt with a diameter of 14 cm, was placed directly on a removable over-water orifice plate. In the CW, there was no cathode or anode, and the anode layer was filled with quartz sand. The constructed wetland- $\text{Fe}_3\text{O}_4/\text{granular}$ activated carbon anode microbial electrolysis cell (CW-FMEC) had a similar configuration to the CW-MEC, but with the upper 1 cm of the GAC anode layer replaced with $\text{Fe}_3\text{O}_4/\text{GAC}$. Water inlets and outlets were set at the bottom and top, and four sampling ports were placed in the middle of the reactor. In the start-up phase, a 25 cm tall canna stem was planted in each wetland. Both electrochemical systems were connected to an external resistor of 1000 Ω via titanium wires as well as to the power supply. In contrast, the CW was not connected to an external circuit. The effective volume of each reactor was about 2.7 L.

2.3. The Experimental Water Characteristics and Water Quality Determination

The simulated nitrate-contaminated groundwater was prepared by adding potassium nitrate (KNO_3), sodium bicarbonate (NaHCO_3), and sodium acetate (CH_3COONa) to 1 L of tap water. The concentrations of NH_4^+-N , $\text{NO}_2^- -\text{N}$, and $\text{NO}_3^- -\text{N}$ were determined via UV spectrophotometry (UV-1100, HACH, Shanghai, China), and the water samples were filtered through a filter membrane with a thickness of 0.45 μm before determination.

Three replicate samples were tested for each sampling to reduce the error. Chemical oxygen demand (COD) was determined according to the standard method.

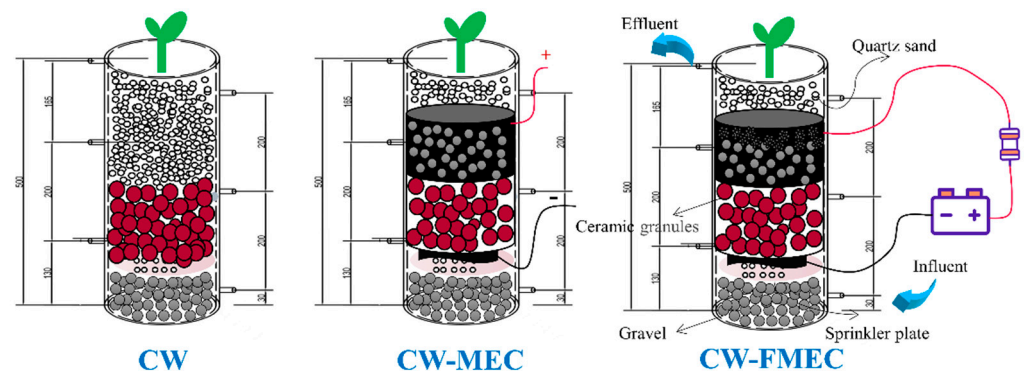


Figure 2. Schematic diagram of reactor structure.

2.4. Wetlands Start-Up and Operation

In the start-up phase, both experimental and control groups were inoculated with anaerobic activated sludge obtained from Longwangzui Municipal Wastewater Treatment Plant, Wuhan, China. In the inoculation process, the activated sludge and constructed simulated wastewater (COD 200 mg/L, NO_3^- -N 40 mg/L, NaHCO_3 50 mg/L) were intermittently fed into the wetland at a volume ratio of 1:1 for a fortnight, with a hydraulic retention time of 48 h. The higher the COD/N, the more rapidly microorganisms grew and biofilm cultivation domesticated and the less the start-up time was. When there was no nitrate in the effluent water, the COD/N ratio slowly reduced, and the wetland changed from intermittent flow to continuous flow and was incubated only with fresh synthetic wastewater, with influent water supplied via a peristaltic pump (BT-100S-1, LEADFLUID, Baoding, China), with a lower inlet and an upper outlet. The hydraulic retention time was maintained at 48 h. The wetland was incubated for two weeks in batches, and the water was fed into the wetland from the peristaltic pump (BT-100S-1, LEADFLUID, Baoding, China). A constant current of 3 mA was applied to both CW-MEC and CW-FMEC. The exterior was wrapped with aluminum foil to avoid the influence of sunlight. In the process of reducing the COD/N ratios, the effluent nitrate concentration was confirmed to be stable under each working condition before continuing to reduce the COD/N ratios. The COD/N ratios were varied by keeping the concentration of the influent NO_3^- -N concentration unchanged while varying that of the influent COD concentration. The reactor was considered to be successfully operational when a grey biofilm could be seen on the electrodes with packing under the condition of 2:1 COD/N ratio and when the nitrate concentration in the effluent remained stable for a week, which took about 30 days. The three COD/N ratios used in the subsequent experiments were 1.5:1, 1:1, and 0.5:1. The system was deemed to be in stable operation when the effluent concentration remained stable for five consecutive days after each change of influent.

2.5. Analytical Methods

The morphology of GAC and Fe_3O_4 /GAC was studied via scanning electron microscopy (SEM, JSM-IT300, Tokyo, Japan). Extracellular polymeric substances (EPS) were chemically extracted from the wetland filler using EDTA method [18]. Polysaccharides and proteins were determined using the Anthrone and Bradford methods, respectively [19,20]. The concentration of c-type cytochromes (c-Cyts) in EPS was determined via a UV-Vis spectrophotometer (UV-1100, HACH, Shanghai, China) [21]. The fillers (ceramic fraction) were collected from the three reactors, rinsed with PBS (0.05 M) and DNA was extracted, then sent to Magigence (Shenzhen, China) for sequencing of the DNA samples using Illuminamiseq/novaseq high-throughput sequencing technology. The purity and concen-

tration of DNA were determined using an ultra-micro spectrophotometer (NanoDrop One, Thermo Fisher, Waltham, MA, USA).

To amplify the 16S rRNA gene, PCR was carried out using primers 338F (5'-ACTCC TACGGGAGGCAGCA-3') and 806R (5'-GGACTACHVGGGTWTCTAAT-3'), selected from the bacterial V3–V4 high variant region [22]. The amplified library was sequenced using the Illumina Nova 6000 sequencing platform (Guangdong Maggian Biotechnology Co., Ltd., Guangzhou, China). The operational taxonomic units (OTUs) were clustered using the usparse method, and sequences with 97% similarity were grouped into identical OTUs [23]. A SmartChip Real-Time PCR System (Wafergen, Fremont, CA, USA)-based high-throughput qPCR chip was utilized to thoroughly examine the quantity and variety of N-related functional genes present in the specimens. The detection status of each gene and Cycle Threshold value in the samples were determined using Canoco software 5. The relative quantitative information of each gene in each sample was then obtained by normalizing the data using 16S rRNA as an internal reference. The absolute quantitative information of the 16S rRNA gene was acquired using the Roche instrument.

3. Results and Discussion

3.1. Characterization of Electrode Material

The morphological characteristics of the anode materials before and after modification were evaluated using scanning electron microscopy (SEM). The SEM images of unmodified GAC showed a regular surface, which is typical of activated carbon, as shown in Figure 3a,b. The SEM images of Fe₃O₄/GAC composites (Figure 3c,d) show that spherical Fe₃O₄ particles with a diameter of about 200 nm were successfully attached to the surface of the GAC, and the surface roughness was significantly improved. Although it has been shown that the binder method clogs the mesopores (2–50 nm) of activated carbon, thus reducing the specific surface area; it promotes the formation of macropores and, at the same time, it can enhance the material's own ability to store charge [24]. Here, the number of macropores (>50 nm) on the surface of the modified material increased significantly. The active bacteria were mainly dependent on the macropores, so this modification facilitated the mass transfer and attachment of bacteria, while the introduction of Fe₃O₄ with good electrical conductivity provided a porous conductive network for electron transfer in the formed biofilm.

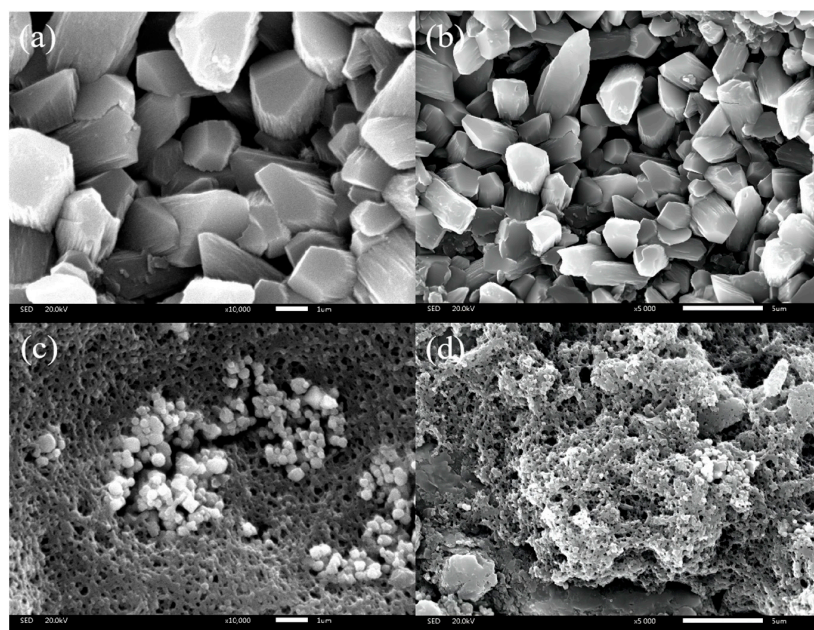


Figure 3. SEM images of GAC: (a) $\times 10,000$ and (b) $\times 5000$; SEM images of Fe₃O₄/GAC: (c) $\times 10,000$ and (d) $\times 5000$.

3.2. Treatment Performance

The nitrogen removal performance of each system was shown in Figure 4. The initial concentration of NO_3^- -N in the wastewater was 39.93 ± 0.57 mg/L, and the current applied to all the electrochemical systems was 3 mA. Under these conditions, the NO_3^- -N effluent concentration of the normal CW decreased to 13.44 ± 0.54 mg/L, 28.60 ± 0.20 mg/L, 32.34 ± 0.44 mg/L, and 34.20 ± 0.30 mg/L when the C: N ratios were 2:1, 1.5:1, 1:1, and 0.5:1, respectively. In the CW-MEC microcosm, the NO_3^- -N effluent concentrations were 11.60 ± 0.50 mg/L, 21.53 ± 0.33 mg/L, 23.28 ± 0.44 mg/L, and 30.12 ± 0.38 mg/L, respectively. NO_3^- -N was not completely removed, where the optimum nitrogen removal efficiency of CW and CW-MEC was $66.38\% \pm 1.37\%$ and $70.98\% \pm 1.54\%$ at a COD/N ratio of 2:1, respectively. And, with the decrease in COD/N, the NO_3^- -N removal performance became worse and worse. In particular, when the COD/N ratio decreased from 2:1 to 1.5:1, the NO_3^- -N removal performance in these two groups showed a cliff-like decline. In contrast, the effluent concentrations at the four stages of CW-FMEC were 4.44 ± 0.46 mg/L, 9.82 ± 0.38 mg/L, 17.38 ± 0.42 mg/L, and 25.12 ± 0.21 mg/L, and the optimum NO_3^- -N removal efficiency at the COD/N ratio of 2:1 reached $88.90\% \pm 1.12\%$, which was significantly higher than that of the other two groups. Interestingly, unlike the other two groups, the NO_3^- -N removal efficiency for CW-FMEC significantly declined when the COD/N ratio decreased from 1.5:1 to 1:1, and the effluent concentration was consistently lower than that of CW and CW-MEC at all four stages, which might be related to the improved utilization of the carbon source by the Fe_3O_4 -modified anode.

In the process of the incomplete reduction of nitrate, NO_2^- -N and NH_4^+ -N accumulated. When acetate was used as a carbon source, a COD/N ratio greater than 3.7 was required for denitrification to proceed more completely [25]. The COD/N ratio in this experiment was consistently in a range that was not sufficient to achieve complete denitrification. At a COD/N ratio of 2:1, the NO_2^- -N content in the CW-MEC microcosm was about 3.13 ± 0.12 mg/L, which was the highest NO_2^- -N concentration observed in this study. It had been reported that the NO_2^- -N concentration increased with the increase in the carbon concentration [26], which is consistent with the results of the present study. CW-MEC accumulated the most NO_2^- -N in either phase, followed by CW and CW-FMEC. Even in the case of the highest accumulation, the NO_2^- -N concentration in CW-FMEC was only 1.37 ± 0.11 mg/L, whereas the NO_2^- -N effluent concentration in CW was twice this value and in CW-MEC it was 2.28 times greater. In this study, NH_4^+ -N concentrations in all three systems were lower. In CW-FMEC, NH_4^+ -N did not accumulate, while in CW-MEC the NH_4^+ -N concentration was up to 0.71 ± 0.09 mg/L; the NH_4^+ -N effluent concentration in CW-MEC was higher than that in CW in each phase.

On the other hand, energy consumption was one of the major costs, so the nitrate nitrogen coulombic reduction rate could be used to evaluate the nitrogen removal performance of individual systems, as shown in Equation (1).

$$u = CV\eta/IT \quad (1)$$

where u was the nitrogen coulomb reduction rate (mg C^{-1}); C was the initial concentration of nitrate in the influent (mg L^{-1}); V was the total volume of the reactor (L); η was the nitrate removal efficiency; I was the applied current (A); and T was the HRT (s).

The results show that all three systems achieved optimal denitrification at a C/N of 2:1 and that the nitrogen degradation coulombic rates for the two systems at the optimum denitrification conditions ($C = 40$ mg/L, $V = 2.7$ L, $I = 3$ mA, and HRT = 48 h) were 0.148 mg/C and 0.185 mg/C, respectively. Among them, the nitrogen degradation coulombic for the removal of nitrate via the CW-FMEC was superior to CW-MEC alone and higher than that reported by other researchers [27–29]. Pratiksha et al. [27] reported a NO_3^- -N coulombic reduction rate of 0.17 mg/C. Zhu et al. [28] reported this value to be 0.031 mg/C in an electrochemical system. Yin et al. [29] reported this value was 0.015 mg/C ($\eta = 95.83\%$) in a heterotrophic/biofilm–electrode autotrophic denitrification

reactor (HAD-BER). Table 1 summarizes the results of other researchers and the results of this study. Based on these results, CW-FMEC not only exhibited high denitrification efficiency but also reduced the accumulation of NO_2^- -N and NH_4^+ -N and reduced energy consumption, which suggests that the anode modified with nano- Fe_3O_4 was favorable for the denitrification of constructed wetland–microbial electrolysis cell.

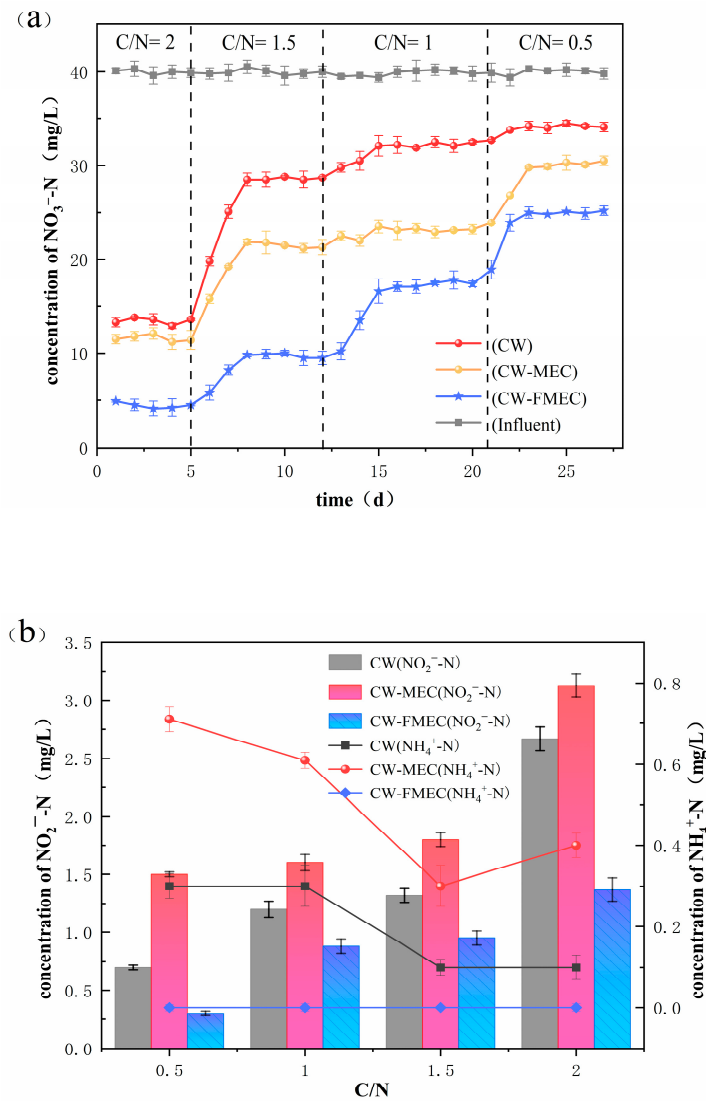


Figure 4. Variation in effluent concentration in control and different electrochemical systems in the experiment ((a). NO_3^- -N; (b). NO_2^- -N and NH_4^+ -N).

Table 1. Summary of previous work conducted by several researchers with a different applied currents.

Reactor Type	Influent Nitrate (mg/L)	Current Intensity (mA)	Removal Efficiencies (%)	Nitrogen Coulomb Reduction Rate (mg/C)
Pratiksha et al. [27]	50	0.233	69.1	0.17
Zhu et al. [28]	35	400	94.2	0.031
Yin et al. [29]	60	60	95.83	0.015
Current study	40	3	88.9	0.185

3.3. COD Removal

The effluent COD of each unit was determined when the effluent from each stage was stable. Figure 5 depicts the COD removal efficiency of individual units at each stage.

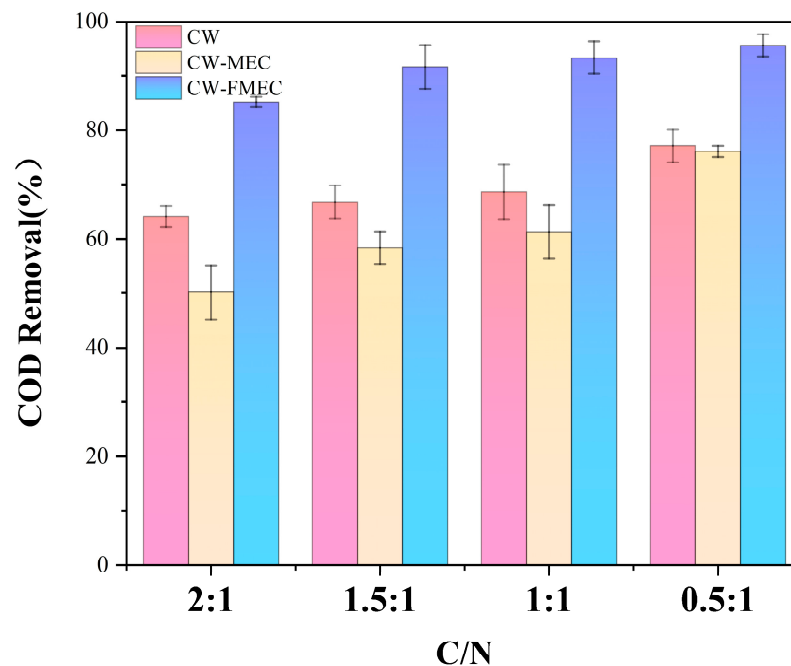


Figure 5. COD removal efficiency of each device at each stage of the process.

When COD/N was varied in the range of 2~0.5, the COD removal rate increased in all three systems, while effluent COD decreased, possibly because the larger the COD/N is, the higher the amount of carbon source added and the higher the content of the effluent containing organic matter that could not be utilized. In addition, CW-FMEC showed the highest COD removal under the same COD/N condition, and the effluent COD was lower than that of CW and CW-MEC. However, the carbon utilization of CW-MEC inversely decreased, and the removal performance of COD became worse compared to CW microcosms. Among them, CW-FMEC removed more than 90% of COD or even up to 95.63% at a COD/N of 1.5~0.5, while CW-MEC removed 14.02% less than CW and 35.02% less than CW-FMEC at a COD/N of 2. Considering the utilization pattern of organic carbon, the overall activity of autotrophic and heterotrophic microorganisms could be determined by combining the utilization rate of organic carbon and the NO_3^- -N removal rate. Combined with the performance of nitrogen removal in each reactor, heterotrophic microorganisms played a dominant role in CW, and the degradation rate of NO_3^- -N decreased with carbon concentration. In the CW-MEC microcosm, both autotrophic and heterotrophic organisms were involved in NO_3^- -N removal, which improved the removal efficiency, but the applied electric field significantly affected the activity of heterotrophic denitrifying microorganisms, which reduced the removal rate of COD removal but positively promoted autotrophic denitrifying microorganisms. Not only was there excellent performance of nitrogen removal but there was also good COD removal in the CW-FMEC; CW-FMEC not only exhibited good denitrification performance but also a good removal effect on COD, which indicates that the activity of heterotrophic and autotrophic denitrifying bacteria in the system was improved after the modification of anode Fe_3O_4 in the CW-FMEC and that the denitrifying autotrophic and heterotrophic bacteria acted synergistically to further enhance nitrogen removal.

3.4. Functional Genes of Different Reactors under Optimal Conditions

To investigate the effect of different systems on microbial metabolism, we quantified the relevant N-functional genes under optimal conditions in the three CW systems, as shown in Figure 6.

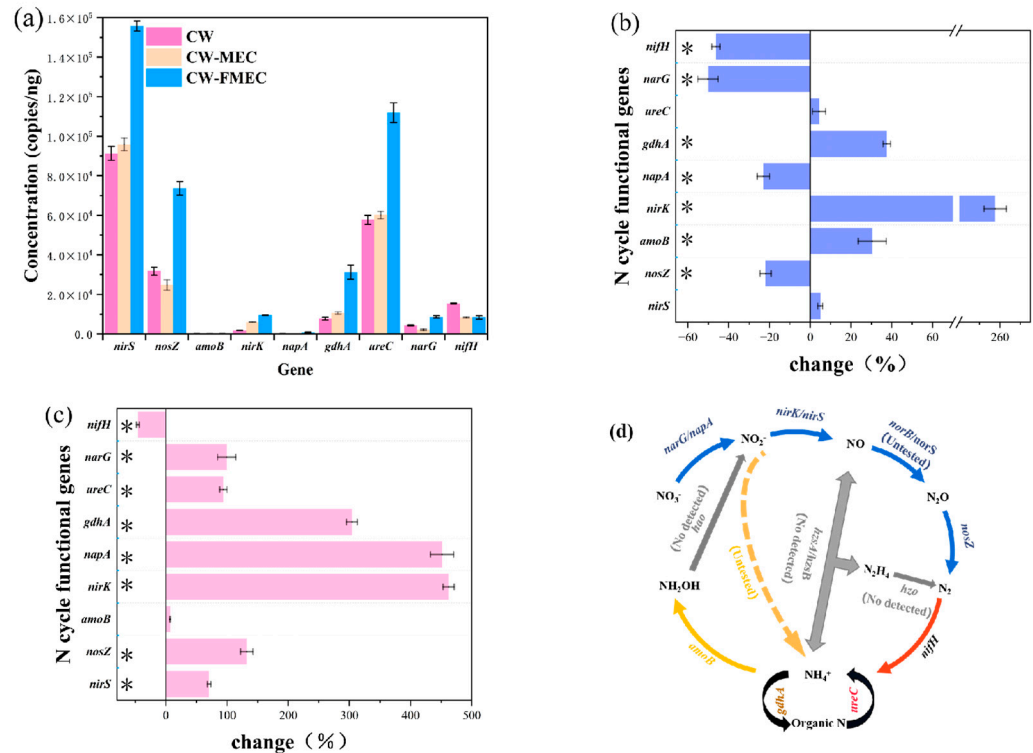


Figure 6. (a) Absolute quantification of N-cycle functional genes; (b) Changes in each N-cycle functional gene in CW-MEC relative to the CW group; (c) Changes in each N-cycle functional gene in CW-FMEC relative to the CW group (* denotes significant difference compared to the control group); (d) Schematic diagram of the N cycle.

Denitrification genes are the basis for the denitrification function of biofilm. In order to gain deeper insights into the effect of the electric field as well as anode modification on the denitrification ability of the system, it was necessary to detect the abundance of denitrification genes in biofilm via qPCR. Figure 6a shows the absolute quantification of genes related to nitrogen cycling such as *narG*, *napA*, *nirS*, *nirK*, and *nosZ* in different reactors. In CW-MEC, the abundance of *napA* and *narG*, encoding nitrate reductase, and *nosZ*, encoding nitrous oxide reductase, decreased, while that of *nirS* and *nirK*, encoding nitrite reductase, both increased. Specifically, the abundance of *napA*, *narG*, and *nosZ* decreased by 22.98%, 50.19%, and 21.88%, while the abundance of *nirS* and *nirK* increased by 4.95% and 257.72%, in CW-MEC compared with CW. Nitrite reductase, encoded by the *nirK* and *nirS* genes, played a crucial rate-limiting role in denitrification. As reductase was located outside the periplasm of the cell, it was more susceptible to environmental factors, suggesting that the imposition of an electric field promoted the expression of nitrite reductase genes [30]. In terms of absolute abundance, the slight increase in *nirS* and *nirK* expression also explained the rate of nitrate removal in the CW-MEC system compared to CW. All key genes associated with the denitrification pathway process were significantly altered in CW-FMEC, with the abundances of *napA*, *narG*, *nirS*, *nirK*, and *nosZ* being significantly higher than in the CW reactor. This indicated that Fe₃O₄-modified, anode-activated carbon based on CW-MEC effectively increased the expression of genes related to the denitrification pathway, thus improving the denitrification effect. Among them, the abundance of *narG*, *nirS*, and *nosZ*, with relatively large absolute abundance, greatly increased by 99.29%, 70.54%, and 132.18%, respectively. The absolute expression

of *nirS*, which played a rate-limiting role and had the highest absolute abundance, was improved from 9.13×10^4 copies/ng DNA to 1.56×10^5 copies/ng DNA. Therefore, it was considered to be the most critical gene affecting reactor performance, which was also in line with the excellent performance of CW-FMEC, which showed the best treatment results accompanied by the lowest NO_2^- -N accumulation.

In addition, combining Figure 6b–d, the application of an electric field and the modified elicitation of $\text{Fe}_3\text{O}_4/\text{GAC}$ led to a reduction in the expression of *nifH*, whereas the only other pathway associated with a source of NH_4^+ was detected for *ureC*, which encodes for urea catabolism. Together with the fact that this study was carried out under the condition of a low COD/N ratio, ammonification respiration was very limited at a low COD/N ratio in environments where denitrification and ammonification coexisted [31]. Hence, the source of NH_4^+ depended mainly on changes in the absolute expression of *nifH*. *AmoB* and *amoA* genes encoding ammonium monooxygenases were related to the destination of NH_4^+ , which played a key role in the nitrification process, and the *gdhA* gene encodes the assimilation of NH_4^+ to glutamate. Although the expression of *amoB* was increased compared to that in CW, the absolute abundance of *amoB* in this study was also relatively small, with no *amoA* detected. Moreover, *hao*, usually considered to be responsible for encoding a gene involved in heterotrophic nitrification, was not detected [32]. On the other hand, the *nxrA* gene encoding nitrite oxidoreductase was not detected here either, suggesting that there was no complete nitrification pathway in any of the three systems. Therefore, the accumulation of NH_4^+ depended mainly on *nifH* and *gdhA*, which were, respectively, related to the source and destination of NH_4^+ . The expression of *nifH* was reduced from 1.54×10^4 copies/ng DNA to 8.29×10^3 copies/ng DNA in CW-MEC compared with that in CW, and that in CW-FMEC was reduced to 8.36×10^3 copies/ng DNA. The expression of *gdhA* increased from 7.74×10^3 copies/ng DNA to 1.06×10^4 copies/ng DNA in CW-MEC, while *gdhA* increased to 3.12×10^4 copies/ng DNA in CW-FMEC— 1.36-fold and 4.03-fold increases, which are also consistent with the fact that NH_4^+ accumulation in CW-MEC was lower than that in CW-FMEC. Here, NH_4^+ accumulation in CW was in between the two, while the expression of *nifH* was reduced to the same level in both electrochemical systems, which also suggests that the change in the expression of *gdhA* played a decisive role in determining NH_4^+ accumulation in the reactor.

3.5. Relative Content of EPS and c-Cyts under Optimal Conditions

EPS has been found to be important in cell adhesion, biorecognition, and electron transfer [33,34], and some of the substances in EPS can accelerate electron transfer and increase denitrifying enzyme activity. The response of biofilm denitrification capacity to electrical stimulation as well as to anodic modification by nano- Fe_3O_4 was determined by measuring the content of extracellular polymers (EPS). Among them, polysaccharides and proteins were the main components of EPS, and the results of polysaccharide and protein content determined upon ceramic packing of each reactor are shown in Figure 7a. Both polysaccharides and proteins upon CW-MEC packing, respectively slightly decreased by 18.6% and 13.1% compared to those on the CW, potentially because some heterotrophic bacteria in the system perceived the applied electric field as a kind of coercion, thus affecting the metabolism, which also corresponds to the lower removal rate of COD.

The contents of protein and polysaccharide in CW-FMEC were significantly higher than those in CW—specifically 67.3% and 63.1% higher than those in CW, respectively—which indicates that the nano- Fe_3O_4 anodic modification caused the microorganisms to secrete more extracellular polymeric substances. Furthermore, the addition of nanomaterials would promote the secretion of microbial extracellular polymers (EPS) and enhance enzyme activity [35], consistent with the best denitrification effect of CW-FMEC in this work.

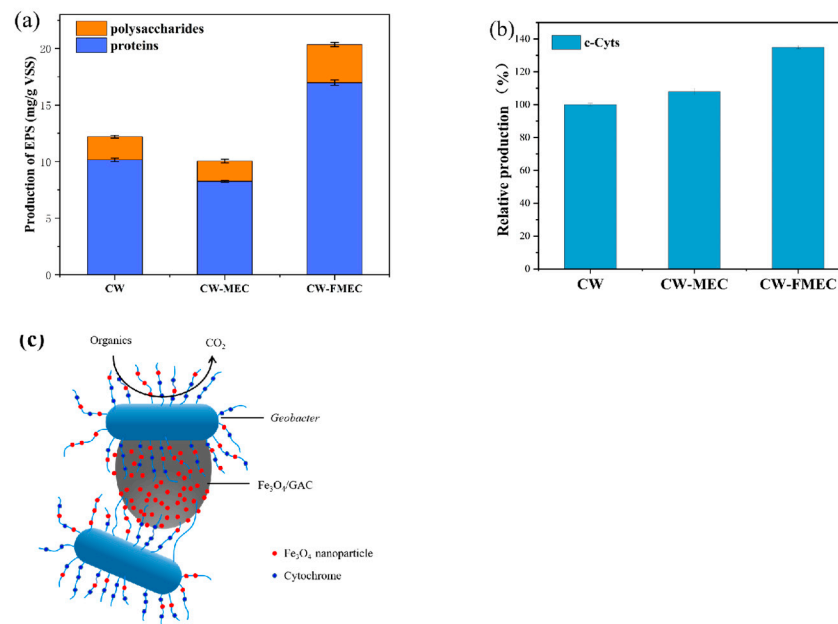


Figure 7. (a) EPS for different reactors, (b) relative content of *c*-Cyts in EPS from different reactors, and (c) schematic diagram of the mechanism of action of Fe₃O₄.

Electrons needed to be transferred to nitrogen oxide reductases such as nitrate reductase (NAR), nitrite reductase (NIR), nitric oxide reductase (NOR), and nitrous oxide reductase (N₂OR) in the denitrification process. This process could be realized by an electron transport chain consisting of complex I (NADH-Co Q reductase), complex III (ubiquinone-cytochrome *c* oxidoreductase) quinone pool, and cytochrome *c* [36,37]. Therefore, increasing the activity of the relevant enzymes and electron transport activity would improve denitrification efficiency and reduce the accumulation of intermediate products (e.g., nitrite and nitrous oxide). To further investigate how the applied electric field and the modification of nano-Fe₃O₄ affect electron transport in the reactor biofilm, the cytochrome *c*-Cyts content in the EPS was measured, as shown in Figure 7b. The results show that, compared with the control group, the relative content of *c*-Cyts in EPS of CW-MEC and CW-FMEC increased by 8% and 35%, respectively, which indicates that electrical stimulation increased the activity of enzymes related to the transfer of electrons and, thus, improved denitrification efficiency. Fe₃O₄/GAC was further modified on this basis, with a better promotion effect and the accumulation of less intermediate products.

Cytochromes acted as iron-containing proteins associated with membranes or diffused into the EPS, which could help establish intercellular connections and facilitate DIET by transferring electrons from electricity-supplying bacteria to various electron acceptors [38,39]. The presence of Fe(III) mimicked the production of *c*-Cyts by bacteria [40,41]. It has also been proved that Fe₃O₄ can act as a substitute for *c*-Cyts to facilitate electron transfer (as shown in Figure 7c) [42].

3.6. Microbial Communities and Structure

To further investigate the differences in the structural composition of the bacterial community in different reactors, microorganisms within the biofilm of each system were studied using 16S rRNA gene sequencing. The main dominant phyla in the three systems were analyzed, as shown in Figure 8. The main dominant phyla were *Proteobacteria*, *Bacteroidetes*, *Chloroflexi*, and *Firmicutes*, all of which played an important role in the nitrogen cycle in natural ecosystems and were abundant in the denitrifying bacterial community in the denitrification system. The *Proteobacteria* phylum had the highest percentage in all three reactors. The common denitrifying bacteria *Thauera*, *Hydrogenophaga*, and *Dechloromonas* were all *Proteobacteria* [43] and, under the influence of the electric field and Fe₃O₄ modi-

fication, the enrichment degree of *Proteobacteria* greatly increased from 36.51% to 45.43% and 82.15%, respectively; it has been reported in the literature that the increase in *Proteobacteria* enrichment is a direct response to the enhancement in denitrification [44]. The total abundance of these dominant phyla basically remained unchanged, indicating that the change in the enrichment degree of *Proteobacteria* was the main factor affecting the denitrification effect.

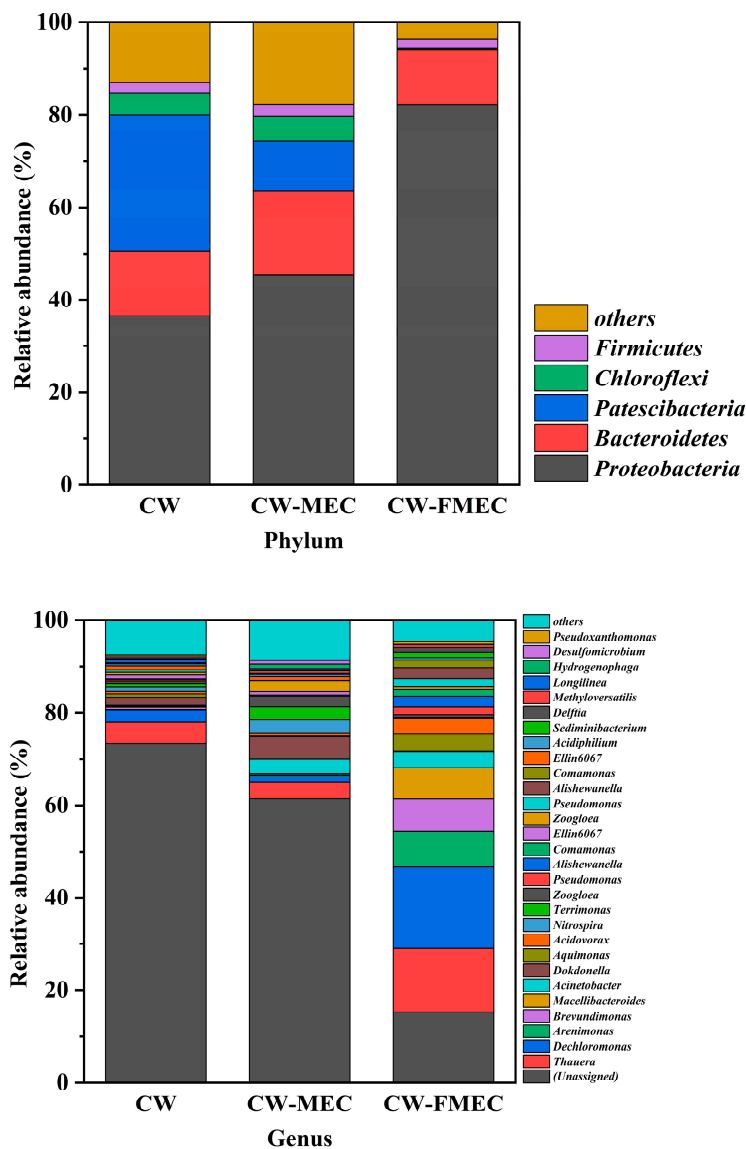


Figure 8. Community structure of different reactors.

At the genus level, *Thauera* and *Dechloromonas* were the dominant genera in CW, *Dokdonella*, *Thauera*, and *Acinetobacter* in CW-MEC, and *Thauera*, *Dechloromonas*, and *Arenimonas* in CW-FMEC. *Thauera* was the most common genus in denitrification systems as it could utilize both organic matter as a carbon source for heterotrophic denitrification and H₂ as an electron donor for hydrogen autotrophic denitrification [45]. *Dokdonella* and *Acinetobacter* were also the two more common genera with denitrification capability [46,47]. Some researchers isolated *Acinetobacter* from a hydrogenotrophic reactor and demonstrated that it played an important role in the denitrification process of hydrogenotrophic denitrification [48]. Compared with CW, the relative abundance of *Thauera* and *Dechloromonas* in CW-MEC slightly decreased by 1.17% and 1.43%, respectively, while that of *Dokdonella* and *Acinetobacter* increased by 3.22% and 3%, respectively. These changes in the abundance of

denitrifying genera also explained the slight enhancement in the performance of CW-MEC relative to CW denitrification.

The most obvious changes in CW-FMEC were manifested by *Thauera*, *Dechloromonas*, and *Arenimonas*, where the relative abundance of *Thauera* and *Dechloromonas* increased by 8.98% and 15.06%, respectively, which is also consistent with a significant increase in the enrichment of the dominant phylum *Proteobacteria*, and the relative abundance of *Arenimonas* increased by 7.61%. *Dechloromonas* was reported to be a bacterium with both heterotrophic denitrification function and hydrogenotrophic denitrification potential [49,50]. The significant increase in the relative abundance of *Thauera* and *Dechloromonas* was one of the key factors for enhancing the nitrogen removal performance of CW-FMEC. It has been reported that *Pseudomonas* can transfer electrons to the anode when stimulated by voltage, while *Arenimonas* can utilize the electrons from the anode to reduce nitrate to improve the system's denitrification efficiency [51]. The enrichment of both genera was increased in CW-FMEC, which was also one of the key factors affecting the removal performance of nitrogen. In addition, *Hydrogenophaga*, another hydrogen autotrophic denitrifying bacterium, also increased from 0.17% in CW to 0.94% in CW-MEC, suggesting that hydrogen was produced in both reactors charged and that *Dechloromonas* might facilitate hydrogenotrophic denitrification. These results showed that heterotrophic denitrification and hydrogen nutrient denitrification coexisted and cooperated in the MEC denitrification system. Furthermore, Fe_3O_4 could enrich *Pseudomonas* and promote its EPS secretion to enhance the denitrification effect at a low COD/N ratio, corresponding to the increased relative abundance of *Pseudomonas* and the good denitrification effect [52].

4. Conclusions

Compared to the CW, the improvement in nitrogen removal performance of CW-MEC at a current of 3 mA and COD/N = 2 was very limited, only from $66.38\% \pm 1.37\%$ to $70.98\% \pm 1.54\%$. On the other hand, the CW-FMEC exhibited an excellent nitrate removal rate ($88.9\% \pm 1.12\%$) without accumulating NO_2^- -N or NH_4^+ -N. All key genes associated with the denitrification pathway were significantly altered in CW-FMEC. The microorganisms were also stimulated to secrete more EPS, and the content of *c*-Cyts increased (35%), which was associated with electron transfer in the denitrification pathway and, consequently, accelerated electron transfer during denitrification. In addition, the abundance of the three dominant denitrifying functional bacteria *Thauera*, *Dechloromonas*, and *Arenimonas* on the filler increased by 8.98%, 15.16%, and 7.61%, respectively. The results demonstrate that the preparation of $\text{Fe}_3\text{O}_4/\text{GAC}$ is a promising method for anode enhancement in CW-MEC.

Author Contributions: Conceptualization, H.Y. and X.T.; Software, S.T.; Validation, H.Y. and Y.H.; Formal analysis, H.Y.; Writing—original draft, H.Y.; Writing—review & editing, S.T., Y.H. and X.T.; Visualization, H.Y.; Funding acquisition, X.T. All authors have read and agreed to the published version of the manuscript.

Funding: This work was funded by the National Natural Science Foundation of China (No. 21806126) and the Fundamental Research Funds for the Central Universities (WUT.2019IVB031).

Data Availability Statement: Data are contained within the article.

Conflicts of Interest: The authors declare no conflicts of interest.

References

1. Juntakut, P.; Snow, D.D.; Haacker, E.M.K.; Ray, C. The long term effect of agricultural, vadose zone and climatic factors on nitrate contamination in the Nebraska's groundwater system. *J. Contam. Hydrol.* **2019**, *220*, 33–48. [[CrossRef](#)] [[PubMed](#)]
2. Sajedi-Hosseini, F.; Malekian, A.; Choubin, B.; Rahmati, O.; Cipullo, S.; Coulon, F.; Pradhan, B. A novel machine learning-based approach for the risk assessment of nitrate groundwater contamination. *Sci. Total Environ.* **2018**, *644*, 954–962. [[CrossRef](#)] [[PubMed](#)]
3. Cayuela, M.L.; Sánchez-Monedero, M.A.; Roig, A.; Hanley, K.; Enders, A.; Lehmann, J. Biochar and denitrification in soils: When, how much and why does biochar reduce N_2O emissions? *Sci. Rep.* **2013**, *3*, 1732. [[CrossRef](#)] [[PubMed](#)]

4. Winkler, M.K.H.; Straka, L. New directions in biological nitrogen removal and recovery from wastewater. *Curr. Opin. Biotechnol.* **2019**, *57*, 50–55. [[CrossRef](#)] [[PubMed](#)]
5. Priya, E.; Kumar, S.; Verma, C.; Sarkar, S.; Maji, P.K. A comprehensive review on technological advances of adsorption for removing nitrate and phosphate from waste water. *J. Water Process Eng.* **2022**, *49*, 103159. [[CrossRef](#)]
6. Wan, D.J.; Wang, J.K.; Shi, Y.H.; Qu, D.; Zhang, J.H. Construction of continuous-flow electro dialysis ion-exchange membrane bioreactor for effective removal of nitrate and perchlorate: Modelling and impact analysis of environmental variables. *Chem. Eng. J.* **2023**, *462*, 142144. [[CrossRef](#)]
7. Wang, Y.; Shen, C.; Tang, Z.B.; Yao, Y.; Wang, X.L.; Park, B. Interaction between particulate fouling and precipitation fouling: Sticking probability and deposit bond strength. *Int. J. Heat Mass Transf.* **2019**, *144*, 118700. [[CrossRef](#)]
8. Singh, S.; Anil, A.G.; Kumar, V.; Kapoor, D.; Subramanian, S.; Singh, J.; Ramamurthy, P.C. Nitrates in the environment: A critical review of their distribution, sensing techniques, ecological effects and remediation. *Chemosphere* **2022**, *287*, 131996. [[CrossRef](#)] [[PubMed](#)]
9. Zekker, I.; Mandel, A.; Rikmann, E.; Jaagura, M.; Salmar, S.; Ghangrekar, M.M.; Tenno, T. Ameliorating effect of nitrate on nitrite inhibition for denitrifying P-accumulating organisms. *Sci. Total Environ.* **2021**, *797*, 149133. [[CrossRef](#)]
10. Wu, H.M.; Zhang, J.; Ngo, H.H.; Guo, W.S.; Hu, Z.; Liang, S.; Fan, J.L.; Liu, H. A review on the sustainability of constructed wetlands for wastewater treatment: Design and operation. *Bioresour. Technol.* **2015**, *175*, 594–601. [[CrossRef](#)]
11. Kill, K.; Grinberga, L.; Koskiahho, J.; Mander, U.; Wahlroos, O.; Lauva, D.; Parn, J.; Kasak, K. Phosphorus removal efficiency by in-stream constructed wetlands treating agricultural runoff: Influence of vegetation and design. *Ecol. Eng.* **2022**, *180*, 106664. [[CrossRef](#)]
12. Zhang, N.; Li, C.Y.; Xie, H.J.; Yang, Y.X.; Hu, Z.; Gao, M.M.; Liang, S.; Feng, K.S. Mn oxides changed nitrogen removal process in constructed wetlands with a microbial electrolysis cell. *Sci. Total Environ.* **2021**, *770*, 144761. [[CrossRef](#)] [[PubMed](#)]
13. Gao, Y.; Zhang, W.; Gao, B.; Jia, W.; Miao, A.J.; Xiao, L.; Yang, L.Y. Highly efficient removal of nitrogen and phosphorus in an electrolysis integrated horizontal subsurface-flow constructed wetland amended with biochar. *Water Res.* **2018**, *139*, 301–310. [[CrossRef](#)] [[PubMed](#)]
14. Song, R.B.; Zhao, C.E.; Gai, P.P.; Guo, D.; Jiang, L.P.; Zhang, Q.; Zhang, J.R.; Zhu, J.J. Graphene/Fe₃O₄ Nanocomposites as Efficient Anodes to Boost the Lifetime and Current Output of Microbial Fuel Cells. *Chem.-Asian J.* **2017**, *12*, 308–313. [[CrossRef](#)] [[PubMed](#)]
15. Logan, B.E.; Rossi, R.; Ragab, A.; Saikaly, P.E. Electroactive microorganisms in bioelectrochemical systems. *Nat. Rev. Microbiol.* **2019**, *17*, 307–319. [[CrossRef](#)] [[PubMed](#)]
16. Xu, S.; Zhou, J.; Shuang, C.; Zhou, Q.; Li, A. Effects of Fe₃O₄ on the denitrification performance of *Pseudomonas stutzeri*. *Sheng Wu Gong Cheng Xue Bao* **2021**, *37*, 3685–3695. [[CrossRef](#)] [[PubMed](#)]
17. Kalantary, R.R.; Farzadkia, M.; Kermani, M.; Rahmatinia, M. Heterogeneous electro-Fenton process by Nano-Fe₃O₄ for catalytic degradation of amoxicillin: Process optimization using response surface methodology. *J. Environ. Chem. Eng.* **2018**, *6*, 4644–4652. [[CrossRef](#)]
18. Keithley, S.E.; Kirisits, M.J. An improved protocol for extracting extracellular polymeric substances from granular filter media. *Water Res.* **2018**, *129*, 419–427. [[CrossRef](#)] [[PubMed](#)]
19. Bradford, M.M. A rapid and sensitive method for the quantitation of microgram quantities of protein utilizing the principle of protein-dye binding. *Anal. Biochem.* **1976**, *72*, 248–254. [[CrossRef](#)]
20. Loewus, F.A. Improvement in Anthrone Method for Determination of Carbohydrates. *Anal. Chem.* **1952**, *24*, 219. [[CrossRef](#)]
21. Li, N.Y.; Quan, X.C.; Zhuo, M.H.; Zhang, X.F.; Quan, Y.P.; Liang, P. Enhancing methanogenesis of anaerobic granular sludge by incorporating Fe/Fe oxides nanoparticles aided with biofilm disassembly agents and mediating redox activity of extracellular polymer substances. *Water Res.* **2022**, *216*, 118293. [[CrossRef](#)] [[PubMed](#)]
22. Guo, X.; Zhong, H.; Li, P.; Zhang, C.J. Microbial communities responded to tetracyclines and Cu(II) in constructed wetlands microcosms with *Myriophyllum aquaticum*. *Ecotoxicol. Environ. Saf.* **2020**, *205*, 111362. [[CrossRef](#)] [[PubMed](#)]
23. Edgar, R.C. UPARSE: Highly accurate OTU sequences from microbial amplicon reads. *Nat. Methods* **2013**, *10*, 996–998. [[CrossRef](#)] [[PubMed](#)]
24. Ho, M.Y.; Khiew, P.S.; Isa, D.; Tan, T.K.; Chiu, W.S.; Chia, C.H.; Hamid, M.A.A.; Shamsudin, R. Nano Fe₃O₄-Activated Carbon Composites for Aqueous Supercapacitors. *Sains Malays.* **2014**, *43*, 885–894.
25. Vrtovsek, J.; Ros, M. Denitrification of groundwater in the biofilm reactor with a specific biomass support material. *Acta Chim. Slov.* **2006**, *53*, 396–400.
26. Chiu, Y.C.; Chung, M.S. Determination of optimal COD/nitrate ratio for biological denitrification. *Int. Biodeterior. Biodegrad.* **2003**, *51*, 43–49. [[CrossRef](#)]
27. Srivastava, P.; Yadav, A.K.; Abbassi, R.; Garaniya, V.; Lewis, T. Denitrification in a low carbon environment of a constructed wetland incorporating a microbial electrolysis cell. *J. Environ. Chem. Eng.* **2018**, *6*, 5602–5607. [[CrossRef](#)]
28. Zhu, M.H.; Fan, J.K.; Zhang, M.L.; Li, Z.Y.; Yang, J.D.; Liu, X.T.; Wang, X.H. Current intensities altered the performance and microbial community structure of a bio-electrochemical system. *Chemosphere* **2021**, *265*, 129069. [[CrossRef](#)] [[PubMed](#)]
29. Yin, H.R.; Lin, X.Y.; Zhao, F.; Pu, Y.; Chen, Y.N.; Tang, X.H. Nano- α -Fe₂O₃ for enhanced denitrification in a heterotrophic/biofilm-electrode autotrophic denitrification reactor. *Water Environ. Res.* **2022**, *94*, e10814. [[CrossRef](#)]
30. Kuypers, M.M.M.; Marchant, H.K.; Kartal, B. The microbial nitrogen-cycling network. *Nat. Rev. Microbiol.* **2018**, *16*, 263–276. [[CrossRef](#)]

31. Yoon, S.; Cruz-García, C.; Sanford, R.; Ritalahti, K.M.; Löffler, F.E. Denitrification versus respiratory ammonification: Environmental controls of two competing dissimilatory $\text{NO}_3^-/\text{NO}_2^-$ reduction pathways in *Shewanella loihica* strain PV-4. *Isme J.* **2015**, *9*, 1093–1104. [[CrossRef](#)] [[PubMed](#)]
32. Xia, L.; Li, X.M.; Fan, W.H.; Wang, J.L. Heterotrophic nitrification and aerobic denitrification by a novel *Acinetobacter* sp. ND7 isolated from municipal activated sludge. *Bioresour. Technol.* **2020**, *301*, 122749. [[CrossRef](#)] [[PubMed](#)]
33. Das, T.; Sehar, S.; Manefield, M. The roles of extracellular DNA in the structural integrity of extracellular polymeric substance and bacterial biofilm development. *Environ. Microbiol. Rep.* **2013**, *5*, 778–786. [[CrossRef](#)] [[PubMed](#)]
34. Deng, S.H.; Li, D.S.; Yang, X.; Zhu, S.B.; Li, J.L. Process of nitrogen transformation and microbial community structure in the Fe(0)-carbon-based bio-carrier filled in biological aerated filter. *Environ. Sci. Pollut. Res.* **2016**, *23*, 6621–6630. [[CrossRef](#)] [[PubMed](#)]
35. Meng, F.G.; Zhang, S.Q.; Oh, Y.; Zhou, Z.B.; Shin, H.S.; Chae, S.R. Fouling in membrane bioreactors: An updated review. *Water Res.* **2017**, *114*, 151–180. [[CrossRef](#)]
36. Liu, S.Q.; Wang, C.; Hou, J.; Wang, P.F.; Miao, L.Z. Effects of Ag NPs on denitrification in suspended sediments via inhibiting microbial electron behaviors. *Water Res.* **2020**, *171*, 115436. [[CrossRef](#)]
37. Berks, B.C.; Ferguson, S.J.; Moir, J.W.; Richardson, D.J. Enzymes and associated electron transport systems that catalyse the respiratory reduction of nitrogen oxides and oxyanions. *Biochim. Biophys. Acta* **1995**, *1232*, 97–173. [[CrossRef](#)]
38. Li, L.; Xu, Y.; Dai, X.H.; Dai, L.L. Principles and advancements in improving anaerobic digestion of organic waste via direct interspecies electron transfer. *Renew. Sustain. Energy Rev.* **2021**, *148*, 111367. [[CrossRef](#)]
39. Liu, T.X.; Luo, X.B.; Wu, Y.D.; Reinfelder, J.R.; Yuan, X.; Li, X.M.; Chen, D.D.; Li, F.B. Extracellular Electron Shuttling Mediated by Soluble *c*-Type Cytochromes Produced by *Shewanella oneidensis* MR-1. *Environ. Sci. Technol.* **2020**, *54*, 10577–10587. [[CrossRef](#)]
40. He, Y.; Guo, J.B.; Song, Y.Y.; Chen, Z.; Lu, C.C.; Han, Y.; Li, H.B.; Hou, Y.A.; Zhao, R. Acceleration mechanism of bioavailable Fe(III) on Te(IV) bioreduction of *Shewanella oneidensis* MR-1: Promotion of electron generation, electron transfer and energy level. *J. Hazard. Mater.* **2021**, *403*, 123728. [[CrossRef](#)]
41. Wan, R.; Chen, Y.G.; Zheng, X.; Su, Y.L.; Huang, H.N. Effect of CO_2 on NADH production of denitrifying microbes via inhibiting carbon source transport and its metabolism. *Sci. Total Environ.* **2018**, *627*, 896–904. [[CrossRef](#)] [[PubMed](#)]
42. Liu, F.; Rotaru, A.-E.; Shrestha, P.M.; Malvankar, N.S.; Nevin, K.P.; Lovley, D.R. Magnetite compensates for the lack of a pilin-associated *c*-type cytochrome in extracellular electron exchange. *Environ. Microbiol.* **2015**, *17*, 648–655. [[CrossRef](#)]
43. Peng, T.; Feng, C.P.; Hu, W.W.; Chen, N.; He, Q.C.; Dong, S.S.; Xu, Y.X.; Gao, Y.; Li, M. Treatment of nitrate-contaminated groundwater by heterotrophic denitrification coupled with electro-autotrophic denitrifying packed bed reactor. *Biochem. Eng. J.* **2018**, *134*, 12–21. [[CrossRef](#)]
44. Tian, Z.J.; Li, G.W.; Xiong, Y.; Cao, X.X.; Pang, H.T.; Tang, W.Z.; Liu, Y.L.; Bai, M.X.; Zhu, Q.H.; Du, C.L.; et al. Step-feeding food waste fermentation liquid as supplementary carbon source for low C/N municipal wastewater treatment: Bench scale performance and response of microbial community. *J. Environ. Manag.* **2023**, *345*, 118434. [[CrossRef](#)] [[PubMed](#)]
45. Zhang, Y.W.; Wei, D.Y.; Morrison, L.; Ge, Z.B.; Zhan, X.M.; Li, R.H. Nutrient removal through pyrrhotite autotrophic denitrification: Implications for eutrophication control. *Sci. Total Environ.* **2019**, *662*, 287–296. [[CrossRef](#)] [[PubMed](#)]
46. Li, M.; Cao, X.W.; Wu, Z.Q.; Li, J.Y.; Cui, Y.; Liu, J.; Li, B.A. Insights on nitrogen and phosphorus removal mechanism in a single-stage Membrane Aeration Biofilm Reactor (MABR) dominated by denitrifying phosphorus removal coupled with anaerobic/aerobic denitrification. *J. Water Process Eng.* **2023**, *52*, 103583. [[CrossRef](#)]
47. Jiang, M.; Wu, Y.T.; Hu, S.Y.; Li, Q.X.; Chen, S.W. Assembled denitrifying consortia for efficient nitrate removal under low-COD/N conditions. *Chem. Eng. J.* **2023**, *460*, 141655. [[CrossRef](#)]
48. Liessens, J.; Vanbrabant, J.; De Vos, P.; Kersters, K.; Verstraete, W. Mixed culture hydrogenotrophic nitrate reduction in drinking water. *Microb. Ecol.* **1992**, *24*, 271–290. [[CrossRef](#)] [[PubMed](#)]
49. Zou, J.T.; Yang, J.Q.; Yu, F.F.; Cai, L.; Li, J.; Ganigu, R. Understanding the role of polyurethane sponges on rapid formation of aerobic granular sludge and enhanced nitrogen removal. *Chem. Eng. J.* **2023**, *460*, 141670. [[CrossRef](#)]
50. Duffner, C.; Holzapfel, S.; Wunderlich, A.; Einsiedl, F.; Schloter, M.; Schulz, S. *Dechloromonas* and close relatives prevail during hydrogenotrophic denitrification in stimulated microcosms with oxic aquifer material. *Fems Microbiol. Ecol.* **2021**, *97*, fiab004. [[CrossRef](#)]
51. Zhang, Z.W.; Han, Y.X.; Xu, C.Y.; Han, H.J.; Zhong, D.; Zheng, M.Q.; Ma, W.W. Effect of low-intensity direct current electric field on microbial nitrate removal in coal pyrolysis wastewater with low COD to nitrogen ratio. *Bioresour. Technol.* **2019**, *287*, 121465. [[CrossRef](#)] [[PubMed](#)]
52. Zhang, F.Y.; Feng, Q.; Chen, Y.; Shi, X.S.; Qin, K.; Lu, M.Y.; Qin, F.; Fu, S.F.; Guo, R.B. Enhancement of biological nitrogen removal performance from low C/N municipal wastewater using novel carriers based on the nano- Fe_3O_4 br. *Bioresour. Technol.* **2022**, *363*, 127914. [[CrossRef](#)] [[PubMed](#)]

Disclaimer/Publisher’s Note: The statements, opinions and data contained in all publications are solely those of the individual author(s) and contributor(s) and not of MDPI and/or the editor(s). MDPI and/or the editor(s) disclaim responsibility for any injury to people or property resulting from any ideas, methods, instructions or products referred to in the content.